MRS Communications (2017), 7, 819–825
© Materials Research Society, 2017
doi:10.1557/mrc.2017.107

MRS Communications

Research Letter

A first-principles study of potassium insertion in crystalline vanadium oxide phases as possible potassium-ion battery cathode materials

Daniel Koch, Vadym V. Kulish, and **Sergei Manzhos,** Department of Mechanical Engineering, National University of Singapore, 9 Engineering Drive 1, Singapore 117576, Singapore

Address all correspondence to Sergei Manzhos at **mpemanzh@nus.edu.sg**

(Received 11 July 2017; accepted 25 September 2017)

Abstract

Four different vanadium oxide phases [α-vanadium pentoxide (V_2O_5), β-V_2O_5, bronze-type vanadium dioxide [VO_2(B)], and rutile-type VO_2 [VO_2(R)])] are investigated from first principles as potential electrode materials for potassium (K) ion batteries. Specifically, insertion energetics and diffusion barriers are computed. These phases are known as promising cathode materials for other types of metal ion batteries. Our results show that the metastable β-V_2O_5 provides the lowest (strongest) insertion energies for K and the lowest diffusion barriers compared with orthorhombic α-V_2O_5, VO_2(B), and VO_2(R). While three of these phases show energetically favorable potassiation and relatively small diffusion barriers, VO_2(R) is predicted to be incapable of electrochemical K incorporation.

Introduction

When it comes to electrochemical energy storage, lithium (Li) ion batteries currently reach the largest market share for portable applications among all battery types. On the other hand, concerns over the longevity of existing Li resources, their distribution and the prospect of upcoming Li utilization in other kinds of technologies started to shift the focus of research toward alternative battery types. The most frequently investigated alternative to Li ions is currently sodium (Na) due to its abundance and relatively low atomic mass as well as good insertion properties for a variety of host materials. As an element almost as abundant (2.14% in the continental crust) as Na (2.36%)[1] and with an even lower standard redox potential (−2.936 V versus Na/Na^+: −2.714 V against SHE) comparable to Li/Li^+ (−3.040 V[2]), the investigation of potassium (K)-based batteries has been gaining interest. Although showing advantageous behavior in terms of standard potential and a generally faster diffusion in electrolytes due to a smaller Stokes radius,[3] there are several obstacles currently preventing a more widespread application of K in batteries, like the large ionic radius of K^+ (1.52 Å radius in crystal octahedral coordination versus Na^+: 1.16 Å versus Al^{3+}: 0.675 Å[4]), which limits the number of suitable host materials capable of accommodating K without significant stresses or volume expansion. Other issues are typical for the alkali metals' safety concerns regarding the use of pure metal anodes due to their reactivity and possible dendrite formation, although the latter issue is believed to be less pronounced than for Li and Na,[5] and a generally lower specific capacity of these technologies due to K's small valence electron number-to-atomic mass ratio compared with other elements such as Li, Na, Mg, or Al.

Possible anodes are relatively well investigated, with carbon based materials being among the most promising candidates for K-ion batteries.[6] Reported cathodic intercalation hosts with possible applications in K-ion batteries span a variety of organic and inorganic compounds from perylenetetracarboxylic dianhydride[7] or poly(anthraquinonyl sulphide)[8] to layered potassium manganates[9] or Prussian blue analogues.[10] Recently reported operation potentials against K metal for Prussian white analogues[11,12] and potassium vanadium phosphate[13] reach up to 3.6 V with capacities up to 142 and 54 mAh/g, respectively, which can reach competitive values relative to other metals. Vanadium oxides recently gained attention as possible electrode materials for advanced electrochemical batteries and especially post-Li batteries due to their ability to incorporate ions of Li, Na, Mg, Al.[14–22] Especially their Li insertion properties as cathodes are extensively documented, with e.g., vanadium dioxide (VO_2) operating at potentials around 2.6 V and vanadium pentoxide (V_2O_5) between 2 and 4 V against Li metal with excellent specific capacities (320 mAh/g for VO_2 and 294 mAh/g for V_2O_5).[14,15]

Promising behavior was also found for the insertion of Na, which is chemically in many regards more similar to K than the second-row element Li. Layered, orthorhombic α-V_2O_5 was shown to reach specific capacities up to 276 mAh/g upon Na insertion and potentials up to 3.8 V against bulk Na.[16] An interesting feature is that pure α-V_2O_5 was shown to exhibit an irreversible phase change during first cycling, forming a stable α'-NaV_2O_5 intercalation compound.[17] Several studies suggest that an increase of the interlayer distance in V_2O_5 increases the

https://doi.org/10.1557/mrc.2017.107 Published online by Cambridge University Press

Na storage capacity due to a better accommodation of the ions between the vanadium oxide sheets and lowering of diffusion barriers.[17,18] The metastable modification β-V_2O_5 differs from the orthorhombic α-V_2O_5 by what can be imagined as a rotation of the $[V_2O_5]_n$ layers around the *a*-direction of the lattice,[23,24] resulting in larger channel-like structures in the *a*–*b* plane, which corresponds to an increase in interlayer distance.

Another well-known Na insertion host is the bronze-type VO_2 [VO_2(B)], studied in several microstructural forms. VO_2(B) microspheres, for example, are reported to have reversible capacities of 383 mAh/g in a voltage range between 3.0 and 0.01 V.[19] Rutile-type, metallic VO_2 [VO_2(R)] on the other hand, the most stable VO_2 phase at elevated temperatures above 68 °C,[25] is less studied with regard to sodium-ion batteries. Existing studies[20–22] suggest a favorable insertion of Na in VO_2(R) and stabilization of the rutile phase by alkali atom insertion, although predicted insertion energies are lower than for Li due to the larger ionic radius of Na. One can therefore surmise that vanadium oxides may be promising for storage of larger-than-Li^+ ions such as K^+.

Since numerous vanadium oxides with different stoichiometries and with distinct phases exist in close proximity in phase space, a systematic experimental study of all possible intercalation compounds and a rationalization of the performance (insertion potentials, capacities) of different phases and of the mechanism of insertion is problematic to achieve. Electronic structure methods on the other hand provide the means to investigate and pre-screen suitable electrode materials and make accurate predictions with regard to the above properties in a systematic way.

The aim of this work is the investigation of a low-concentration K insertion into several crystalline vanadium oxide phases, of K binding energies (indicative of possible voltages), preferred interstitial sites and diffusion barriers (indicative of rate performance) as well as changes in electronic structure using density functional theory (DFT). We chose the above mentioned four common vanadium oxides for this study: α-V_2O_5, VO_2(B), β-V_2O_5, and VO_2(R). The behavior of these compounds, previously compared for Li, Na, Mg, and Al storage,[21,22] upon K insertion is here studied with the same computational setup to draw comparisons. K insertion in α-V_2O_5 was already treated theoretically by Carrasco[26] using Perdew–Burke–Ernzerhof (PBE) and optPBE-van der Waals (vdW) functionals in the dilute regime to obtain insertion voltages and diffusion barriers, leading to intermediate values for both properties ranging between the tested alkali and alkaline-earth metals. K insertion into pencil-shaped VO_2(R) nanostructures was studied experimentally,[20] suggesting a less favorable K intercalation compared with Li and Na.

K insertion into the crystalline vanadium oxide phases is modeled using DFT and dispersion-corrected DFT in this work, employing the PBEsol functional (GGA) with a plane wave basis and the projector augmented wave method. The complete computational details are provided in the Supplementary Material. Specifically, the computed quantities include binding energies, E_b, of K to the host structure versus the cohesive energy of K (related to expected voltage), diffusion barriers, as well as densities of states (DOS) and spin density differences, see Supplementary Material for more details.

K insertion energetics

For each of the phases [α-V_2O_5, VO_2(B), β-V_2O_5, and VO_2(R)], there are several non-equivalent insertion sites for metal ions, as shown in Fig. 1. These sites differ by coordination number and bond distances and therefore deliver varying binding energies as can be seen in Table I, where besides E_b [Eq. (1) in the Supplementary Material] as well as Bader charges on K and strain energies [Eq. (2) in the Supplementary Material] are tabulated. Negative values of E_b correspond to thermodynamically preferred insertion of K atoms versus formation of bulk K and vice versa, see Supplementary Material.

α-V_2O_5 (space group *Pmmn*) consists of interconnected VO_5 pyramids forming two shifted ladders in crystallographic *a*-direction. In the case of the α phase, insertion takes place into the sixfold oxygen coordinated site denoted by *S*1. The K–O bond lengths are 2.59–2.63 Å within the trigonal-prismatic coordination polyhedron. Other possible minimum-energy sites in α-V_2O_5 identified in a previous investigation by our group for other alkali metals,[21] denoted by *S*2 and *S*3 in Fig. 1, were not found to represent stable minima in the case of K. The most favorable insertion site in β-V_2O_5 (space group *Cmcm*) is found to be the fivefold coordinated *S*1 position, while binding energy is slightly weaker for the fourfold coordinated *S*2 site due to a smaller coordination polyhedron volume. The K–O distances for *S*1 and *S*2 are 2.56–2.63 and 2.48–2.67 Å, respectively. For VO_2(B) (space group *C*2/*m*), consisting of stacked double layers of connected VO_6 octahedra, the eightfold coordinated *C* insertion site (K–O distances of 2.60–2.88 Å) is the only stable one, while K in the additionally tested *A*1 and *A*2 positions move toward *C* due to high lattice strains. The common insertion sites in VO_2(R) (space group $P4_2/mnm$) are located within the channel-like structures along the crystallographic *c*-direction, which are spanned by edge-connected VO_6 octahedra, and are either octahedrally (*oct*) or tetrahedrally (*tet*) coordinated by oxygen. However, binding energies for both sites are positive with regard to bulk K, which implies that metal plating would be favored against K insertion. As can be seen in Table I, strain energy in potassiated VO_2(R) is remarkably high due to the pronounced lattice distortions upon insertion of the large K ion into the relatively narrow channels causing an inhibited solute–host overlap and low electronic K-VO_2 binding contributions, which are not able to counter the large positive strain energy. Ref. [20] studied Li, Na, and K interactions with nanopencils of VO_2(R). There were not able to confirm insertion into the bulk of the material and only suggested that with all Li, Na, and K, there is evidence of vanadium reduction. This can mean interfacial storage rather than insertion. Our calculation therefore provides additional insight into K storage in this material.

To demonstrate the connection between decreasing binding energies and increasing sterical hindrance by narrowing of the

https://doi.org/10.1557/mrc.2017.107 Published online by Cambridge University Press

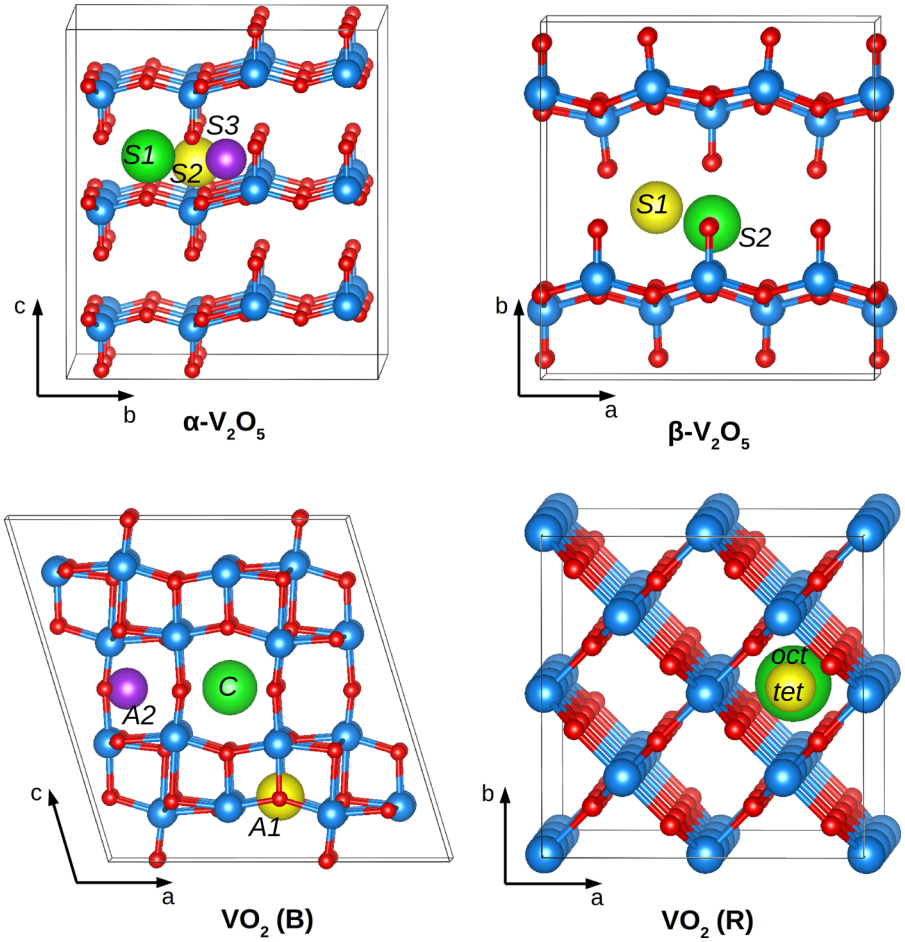


Figure 1. α-V_2O_5, β-V_2O_5, VO_2(B), and VO_2(R) (from top left to bottom right panel) supercells with possible insertion sites. The red spheres denote O, the blue spheres V positions, possible K insertion sites are denoted by green, yellow, and purple spheres and their designations are given. Crystallographic directions along front face of cell are indicated.

channel sizes in different vanadium oxide compounds, the (favored) channels can be approximated as cylindrical tubes with the maximum radius which do not include any ion center and can be fitted into the crystal structures. The radii of those imaginary cylindrical cross-sections are 1.97 Å in β-V_2O_5 and 1.92 Å in α-V_2O_5 *a*-directions, as well as 1.69 Å in VO_2(B) *b*- and 1.61 Å in VO_2(R) *c*-direction. These radii can be taken as a relative measure for the available space for any intercalant in the pristine structures and provide a reasonable selection of diffusion directions to scan for the computation of diffusion barriers. As one can see, the channel radii correlate with the K binding energies in the investigated vanadia compounds.

From the Bader charges listed in Table I, it can be observed that charge transfer between solute and host is most pronounced for insertion in β-V_2O_5, followed by α-V_2O_5, VO_2(B), and VO_2(R). The Bader charges correlate with the difference of binding and corresponding strain energies, since this combined quantity provides a measure for the energy gain caused by solute–host orbital overlap. In general, it can be stated that the K insertion is predicted to be energetically most favorable in β-V_2O_5 from all considered phases, due to the small lattice strain contributions and moderate displacements enhanced by the large interlayer spacing. In terms of binding energies, VO_2(B) and α-V_2O_5 show a relatively large drive to insertion as well, with lower lattice strains and stronger solute–host binding in the case of orthorhombic V_2O_5 whose K binding energy is close to that of β-V_2O_5. The VO_2(R) lattice, however, is subjected to large deformations upon K insertion, resulting in positive binding energies, so that no intercalation reaction of this phase is predicted at this level of theory.

Our results for α-V_2O_5 can be compared with a recent study by Carrasco[26] using PBE and optPBE-vdW functionals, which reported insertion energies of −3.11 eV with PBE and −3.33 eV with the dispersion-corrected optPBE-vdW functional, which are in decent agreement with our value of −2.89 eV. We note that vdW corrections tend to increase the binding strength artificially, especially for the cases where atoms are fully ionized, like Li, Na, Mg, or K insertion, as dispersion corrections like the Grimme scheme are not defined for such cases.[27–29] The calculations presented above did not

https://doi.org/10.1557/mrc.2017.107 Published online by Cambridge University Press

Table I. Binding energies per K atom, Bader charges of K, and strain energy upon single-atom insertion in α-V_2O_5, β-V_2O_5, VO_2(B), and VO_2(R) supercells and the possible insertion sites in each crystal structure. The formula index x corresponds to a small number at the dilute limit, formally x is equal to 0.03 [VO_2(R) and VO_2(B)], 0.06 (α-V_2O_5), and 0.01 (β-V_2O_5).

Phase	Site	E_b [eV]	q_{Bader}(K) [e]	E_{strain} [eV]
α-$K_xV_2O_5$	*S*1	−2.89	+0.83	+0.51
	*S*2	Not stable		
	*S*3	Not stable		
β-$K_xV_2O_5$	*S*1	−3.07	+0.86	+0.45
	*S*2	−3.01	+0.87	+0.59
K_xVO_2(B)	*A*1	Not stable		
	C	−2.54	+0.81	+0.29
	*A*2	Not stable		
K_xVO_2(R)	*oct*	+2.43	+0.72	+2.53
	tet	+2.43	+0.72	+2.49

employ vdW corrections, to treat on the same footing layered and non-layered phases. We have also performed calculations with Grimme dispersion corrections. The results are given in Supplementary Material Tables S1 and S2. The inclusion of dispersion corrections changes E_b for the layered phases by <0.1 eV. However, it changes E_b for the non-layered phases by up to 0.3 eV while making lattice constants less accurate for both layered and non-layered phases.

Electronic structure analysis

After the lowest energy insertion sites in all four compounds were found, the changes in electronic structure upon insertion into these preferential positions were analyzed. As can be seen from the DOS of all four phases shown in Fig. 2, pristine α-V_2O_5 and β-V_2O_5 are semiconducting materials with substantial band gaps of ∼1.7 eV, while pristine VO_2(R) and VO_2(B) are predicted to be metallic.[22] The net magnetic moments of the V_2O_5 supercells are zero, while in both VO_2 phases all unpaired electron spins on vanadium are ordered within the supercell, which has a net magnetic moment corresponding to one unpaired electron per vanadium atom, as expected. The valence bands of the V_2O_5 have mostly O 2*p* character, while the conduction bands consist primarily of V 3*d* contributions. For the pristine VO_2, V 3*d* fractions start to dominate below the Fermi level, corresponding to a partial occupation of V^{4+} *d* orbitals and being the major contribution to above-Fermi energy states as well.

Upon insertion of K, K 4*s* electrons, lying significantly above the Fermi levels of the pristine materials, transfer to lower, previously unoccupied V *d* states, causing a shift in Fermi levels. In V_2O_5 phases, the occupied vanadium states lie within the band gap, pinning the corresponding Fermi level between newly occupied and conduction band states. To better understand which states the newly inserted K valence electron occupies, spin density difference plots are shown in Fig. 3. As can be seen for α-V_2O_5 in the top left panel, the additional valence electron is donated and delocalized over a V–O–V bond in crystallographic *b*-direction with both vanadium atoms bearing parallel magnetic moments of ∼0.5 μ_B, coupled over the bridging O atom with antiparallel magnetic moment. This situation is similar to what was previously found for α'-NaV_2O_5, which can be formed upon Na insertion into the α-V_2O_5 phase: electrons in the sodiated α' compound are delocalized over the V–O–V rungs of the α-V_2O_5 ladders and magnetically coupled among each other.[30–32] Since the K concentration is far below 12.5%, spin coupling between the rungs cannot be observed, but the electron delocalization across the rung was found in a similar manner. In β-V_2O_5, the rungs of the ladders lie in crystallographic *c*-direction and a similar situation as for the α phase can be observed in the right panel of Fig. 3. The closest V–O–V bond in positive *b*-direction carries an overall magnetic moment of ∼1.0 μ_B, with the spins on two vanadium centers being coupled by an opposite spin on the oxygen.

In the case of the metallic VO_2, inserted electrons are transferred into unoccupied above-Fermi energy vanadium *d* states of the pristine lattice, accompanied by a small shift in Fermi energy. Since spins in both these VO_2 phases are coupled ferromagnetically, leading to an initially spin polarized lattice, the evaluation of spin density differences is not instructive in these cases. The eigenstates of the potassiated VO_2(B) and VO_2(R) phases around the Fermi level are delocalized over large parts of the supercell, so no specific localized K–V electron transfer could be observed for these vanadium dioxides.

Diffusion barriers

In Fig. 4, the diffusion barriers of K in α-V_2O_5, β-V_2O_5, and VO_2(B) along the lowest barrier directions are shown. The preferred diffusion directions were chosen by largest channel size and other reasonable diffusion directions were also tested by nudged elastic band calculations along those competing channels, which were not found to provide lower barriers. VO_2(R) is omitted here, since no stable intercalation phase was found. The relative energies were calculated on a path between two equivalent minimum-energy insertion sites. K diffusion in these vanadium pentoxides was found to occur preferentially along the crystallographic *a*-direction along the ladders. Starting and end points of the diffusion paths are two *S*1 sites in both structures. In the case of β-V_2O_5, the diffusion path includes the *S*2 site (see Fig. 1) as local minimum at half of the distance between two *S*1 sites, while in α-V_2O_5 a maximum-energy configuration lies between the two minima (see Fig. 4). The K diffusion barrier in the β phase is only 0.07 eV between *S*1 and *S*2 and consequently 0.01 eV between the *S*2 and *S*1 sites. This low diffusion barrier can be explained by pronounced lattice distortions at both minima (*S*1 and *S*2), which locally widen the channel size and makes diffusion

https://doi.org/10.1557/mrc.2017.107 Published online by Cambridge University Press

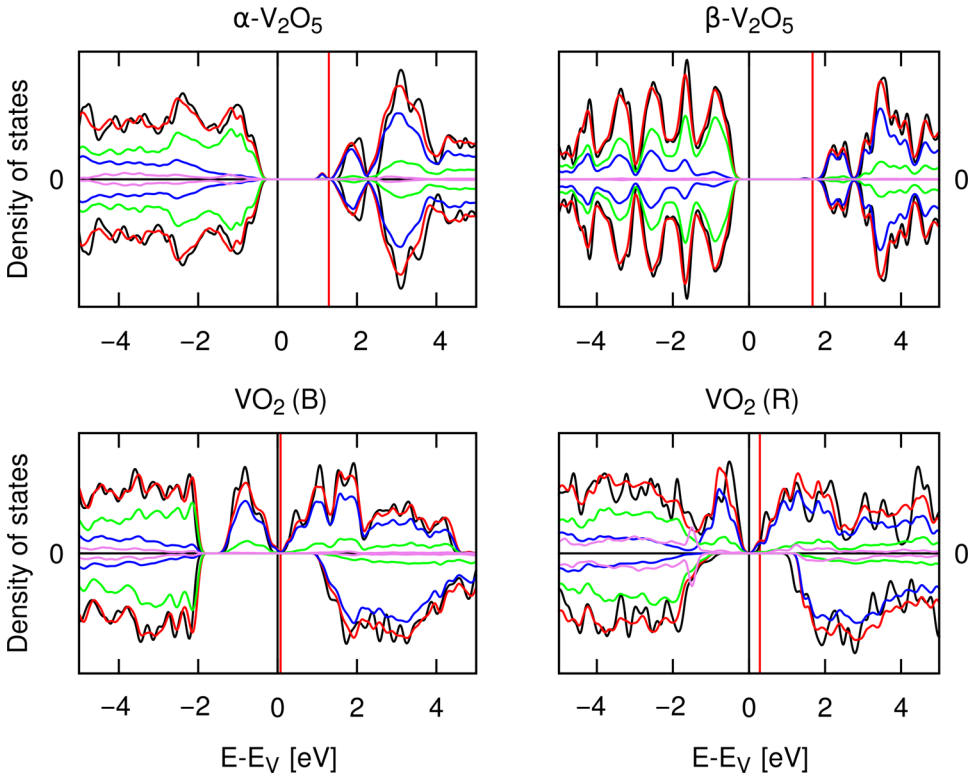


Figure 2. DOS for pristine (black line) and potassiated (red line) α-V_2O_5, β-V_2O_5, VO_2(B), and VO_2(R) (from top left to bottom right) for the lowest-energy K insertion sites. Positive and negative DOS values indicate up and down spin, respectively. Energies are relative to valence band edge (or Fermi level of the pristine compound in the case of rutile- and bronze-type VO_2). The relative positions Fermi levels are indicated by vertical lines. The partial densities of states for the three atomic species are indicated in blue (vanadium), green (oxygen), and violet (potassium, scaled by a factor of 100 for better visibility) in every panel.

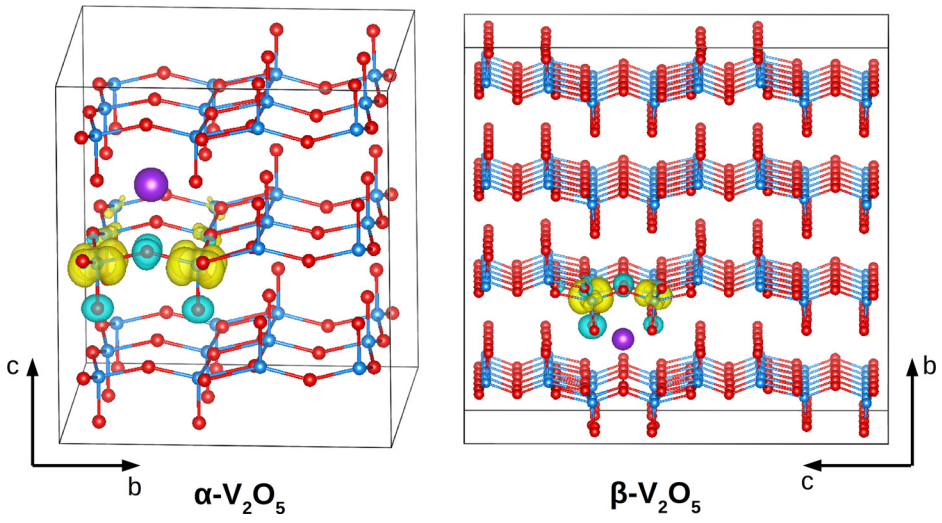


Figure 3. Spin density difference plots of α-V_2O_5 (left) and β-V_2O_5 (right) after K (purple) insertion into the lowest insertion energy sites. V positions are denoted by blue, O positions by red spheres. Residual spin-up and -down densities are represented in yellow and turquoise, respectively.

https://doi.org/10.1557/mrc.2017.107 Published online by Cambridge University Press

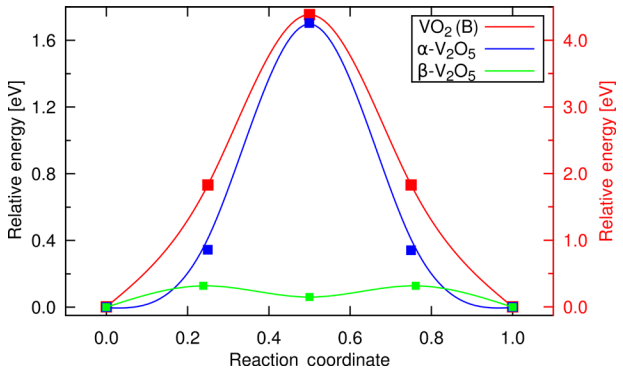


Figure 4. Barriers for the diffusion of K in $K_{0.03}VO_2$(B), α-$K_{0.06}V_2O_5$, β-$K_{0.01}V_2O_5$ between two equivalent lowest energy insertion sites. The right ordinate (labels in red) refers to VO_2(B) (red curve), the left ordinate to all other curves.

almost barrier-less compared with the other compounds. As a measure for atomic displacements, the sum of Euclidean distances between equivalent atomic positions in pristine and strained structures can be used, which is 0.96 Å in the case of β-V_2O_5 (*S*1 site) compared with 0.78 Å in α-V_2O_5 and 0.30 Å in VO_2(B). Considering similar magnitudes of E_{strain} in α, β, and bronze phases (Table I), this means that the β phase is softer and therefore more accommodative of the K in the transition state. We did repeat the calculation with a β-V_2O_5 supercell doubled in each direction, as described in the Supplementary Material, yet the barrier remained similarly low. We chose the PBEsol method as providing a good description of all four phases, pure as well as under the insertion of Li, Na, Mg, and Al[21,22]; however, it might fail in the presence of a larger K ion. To check for a possible method failure in describing the weakly vdW-bound layers in β-V_2O_5, we also performed calculations with Grimme corrections as described in Supplementary Material, and the barrier was still on the order of 0.1 eV. A comparison of diffusion barriers in β-V_2O_5 with and without D2 corrections is given in Supplementary Material Fig. S1. Due to the increased strain energy caused by additional O–O interactions with dispersion corrections included, the intermediate *S*2 site is not a local minimum anymore but represents the transition state of the *S*1-to-*S*1 diffusion.

In the α phase, the diffusion barrier is 1.70 eV, which is consistent with former investigations on insertions of other metals (Na, Mg, Al) in α-V_2O_5, whose diffusion barriers in the same crystallographic direction were of the same order of magnitude.[21] These results are also in good agreement with the previously mentioned existing literature, suggesting a less hindered diffusion in V_2O_5 with increasing interlayer distance and therefore widened diffusion channels along the ladders.

The diffusion barrier between two *C* sites in VO_2(B) was found to be 4.38 eV, a value significantly higher than for α- and β-V_2O_5, making diffusion prohibitive at room temperature. This can be explained by the tetragonally coordinated (i.e., there is a significant change in coordination between the minimum and the transition state, which is known to lead to high barriers), distorted configuration at the barrier maximum (center of the diffusion path), for which increasing strain (E_{strain} = +2.27 eV at the path maximum) and insufficient overlap in the low-coordinated environment result in a large relative image energy. This is contrasted by the transition states in the V_2O_5 phases with less pronounced distortions and therefore lower strain energies as well as enhanced K-VO_x binding.

Conclusions

This study provides a comparative computational evaluation of vanadia compounds of different phases and stoichiometries [α-V_2O_5, β-V_2O_5 as well as VO_2(R) and VO_2(B)] with the same computational setup. We found that β-V_2O_5 is expected to deliver the highest initial voltages (3.07 V) under potassiation (corresponding to the strongest K binding energies) of all investigated phases. The preferential insertion of K into the β-V_2O_5 phase can be explained by its large interlayer distance (~4.2 Å shortest interlayer V–O distance in *b*-direction compared with ~2.7 Å along *c* in α-V_2O_5), providing large interstitial sites to incorporate the K^+ ion. This wide interlayer spacing further gives rise to the lowest diffusion barrier among the phases. Increasing strain energy is causing a decrease in binding energy strength and in predicted initial voltages upon potassiation in α-V_2O_5 (2.89 V), VO_2(B) (2.54 V), and finally VO_2(R) (−2.43 V, i.e., inactive). The diffusion barriers in orthorhombic V_2O_5 and VO_2(B) are higher than for β-V_2O_5, due to the steric hindrance and higher strain energies along the diffusion path. These results can be used to rationally select crystalline vanadia materials for future in-depth investigations at other states of charge.

Supplementary material

The supplementary material for this article can be found at https://doi.org/10.1557/mrc.2017.107.

Acknowledgments

This work was supported by the Ministry of Education of Singapore (Grant No. MOE2015-T2-1-011).

References

1. K.H. Wedepohl: The composition of the continental crust. *Geochim. Cosmochim. Acta* **59**, 1217 (1995).
2. Y. Marcus: Thermodynamic functions of transfer of single ions from water to nonaqueous and mixed solvents: part 3—standard potentials of selected electrodes. *Pure Appl. Chem.* **57**, 1129 (1985).
3. S. Komaba, T. Hasegawa, M. Dahbi, and K. Kubota: Potassium intercalation into graphite to realize high-voltage/high-power potassium-ion batteries and potassium-ion capacitors. *Electrochem. Commun.* **60**, 172 (2015).
4. R.D. Shannon: Revised effective ionic radii and systematic studies of interatomic distances in halides and chalcogenides. *Acta Crystallogr. Sect. A* **32**, 751 (1976).
5. A. Eftekhari, Z. Jian, and X. Ji: Potassium secondary batteries. *ACS Appl. Mater. Interfaces* **9**, 4404 (2017).
6. K. Share, A.P. Cohn, R. Carter, B. Rogers, and C.L. Pint: Role of nitrogen-doped graphene for improved high-capacity potassium ion battery anodes. *ACS Nano* **10**, 9738 (2016).

https://doi.org/10.1557/mrc.2017.107 Published online by Cambridge University Press

7. Y. Chen, W. Luo, M. Carter, L. Zhou, J. Dai, K. Fu, S. Lacey, T. Li, J. Wan, X. Han, Y. Bao, and L. Hu: Organic electrode for non-aqueous potassium-ion batteries. *Nano Energy* **18**, 205 (2015).
8. Z. Jian, Y. Liang, I.A. Rodríguez-Pérez, Y. Yao, and X. Ji: Poly(anthraquinonyl sulfide) cathode for potassium-ion batteries. *Electrochem. Commun.* **71**, 5 (2016).
9. C. Vaalma, G.A. Giffin, D. Buchholz, and S. Passerini: Non-aqueous K-ion battery based on layered $K_{0.3}MnO_2$ and hard carbon/carbon black. *J. Electrochem. Soc.* **163**, A1295 (2016).
10. C.D. Wessells, S.V. Peddada, R.A. Huggins, and Y. Cui: Nickel hexacyanoferrate nanoparticle electrodes for aqueous sodium and potassium ion batteries. *Nano Lett.*. **11**, 5421 (2011).
11. L. Xue, Y. Li, H. Gao, W. Zhou, X. Lü, W. Kaveevivitchai, A. Manthiram, and J.B. Goodenough: Low-cost high-energy potassium cathode. *J. Am. Chem. Soc.* **139**, 2164 (2017).
12. X. Wu, Z. Jian, Z. Li, and X. Ji: Prussian white analogues as promising cathode for non-aqueous potassium-ion batteries. *Electrochem. Commun.* **77**, 54 (2017).
13. J. Han, G.-N. Li, F. Liu, M. Wang, Y. Zhang, L. Hu, C. Daiab, and M. Xu: Investigation of $K_3V_2(PO_4)_3$/C nanocomposites as high-potential cathode materials for potassium-ion batteries. *Chem. Commun.* **53**, 1805 (2017).
14. S. Lee, X.-G. Sun, A.A. Lubimtsev, X. Gao, P. Ganesh, T.Z. Ward, G. Eres, M.F. Chisholm, S. Dai, and H.N. Lee: Persistent electrochemical performance in epitaxial VO_2(B). *Nano Lett.* **17**, 2229 (2017).
15. H. Yamada, K. Tagawa, M. Komatsu, I. Moriguchi, and T. Kudo: High power battery electrodes using nanoporous V_2O_5/carbon composites. *J. Phys. Chem. C* **111**, 8397 (2007).
16. V. Raju, J. Rains, C. Gates, W. Luo, X. Wang, W.F. Stickle, G.D. Stucky, and X. Ji: Superior cathode of sodium-ion batteries: orthorhombic V_2O_5 nanoparticles generated in nanoporous carbon by ambient hydrolysis deposition. *Nano Lett.* **14**, 4119 (2014).
17. D. Muller-Bouvet, R. Baddour-Hadjean, M. Tanabe, L.T.N. Huynh, M.L. P. Le, and J.P. Pereira-Ramos: Electrochemically formed α'-NaV_2O_5: a new sodium intercalation compound. *Electrochim. Acta* **176**, 586 (2015).
18. S. Tepavcevic, H. Xiong, V.R. Stamenkovic, X. Zuo, M. Balasubramanian, V.B. Prakapenka, C.S. Johnson, and T. Rajh: Nanostructured bilayered vanadium oxide electrodes for rechargeable sodium-ion batteries. *ACS Nano* **6**, 530 (2012).
19. B. Yan, X. Li, Z. Bai, L. Lin, G. Chen, X. Song, D. Xiong, D. Lic, and X. Sun: Superior sodium storage of novel VO_2 nano-microspheres encapsulated into crumpled reduced graphene oxide. *J. Mater. Chem. A* **5**, 4850 (2017).
20. I. Mjejri, N. Etteyeb, S. Somrani, and F. Sediri: Tetragonal pencil-like VO_2(R) as electrode materials for high-performance redox activities. *Ceram. Int.* **42**, 6121 (2016).
21. V. Kulish, and S. Manzhos: Comparison of Li, Na, Mg and Al-ion insertion in vanadium pentoxides and vanadium dioxides. *RSC Adv.* **7**, 18643 (2017).
22. V.V. Kulish, D. Koch, and S. Manzhos: Ab initio study of Li, Mg and Al insertion into rutile VO_2: fast diffusion and enhanced voltages. Submitted to *Phys. Chem. Chem. Phys.* **19**, 22538 (2017). doi: 10.1039/C7CP04360K.
23. B. Zhou, H. Shi, R. Cao, X. Zhang, and Z. Jiang: Theoretical study on the initial stage of a magnesium battery based on a V_2O_5 cathode. *Phys. Chem. Chem. Phys.* **16**, 18578 (2014).
24. C. Delmas, H. Cognac-Auradou, J.M. Cocciantelli, M. Ménétrier, and J. P. Doumerc: The $Li_xV_2O_5$ system: an overview of the structure modifications induced by the lithium intercalation. *Solid State Ion.* **69**, 257 (1994).
25. F.J. Morin: Oxides which show a metal-to-insulator transition at the Neel temperature. *Phys. Rev. Lett.* **3**, 34 (1959).
26. J. Carrasco: Role of van der Waals forces in thermodynamics and kinetics of layered transition metal oxide electrodes: alkali and alkaline-earth ion insertion into V_2O_5. *J. Phys. Chem. C* **118**, 19599 (2014).
27. M.A. Sk, and S. Manzhos: Exploring the sodium storage mechanism in disodium terephthalate as anode for organic battery using density-functional theory calculations. *J. Power Sources* **324**, 572 (2016).
28. Y. Chen, and S. Manzhos: A comparative computational study of lithium and sodium insertion into van der Waals and covalent tetracyanoethylene (TCNE)-based crystals as promising materials for organic lithium and sodium ion batteries. *Phys. Chem. Chem. Phys.* **18**, 8874 (2016).
29. Y.Y. Zhang, Y.Y. Sun, S.X. Du, H.-J. Gao, and S.B. Zhang: Organic salts as super-high rate capability materials for lithium-ion batteries. *Appl. Phys. Lett.* **100**, 091905 (2012).
30. H. Smolinski, C. Gros, W. Weber, U. Peuchert, G. Roth, M. Weiden, and C. Geibel: NaV_2O_5 as a quarter-filled ladder compound. *Phys. Rev. Lett.* **80**, 5164 (1998).
31. A.N. Yaresko, V.N. Antonov, H. Eschrig, P. Thalmeier, and P. Fulde: Electronic structure and exchange coupling in α'-NaV_2O_5. *Phys. Rev. B* **62**, 15538 (2000).
32. X. Ming, H.-G. Fan, Z.-F. Huang, F. Hu, C.-Z. Wang, and G. Chen: Magnetic gap in Slater insulator α'-NaV_2O_5. *J. Phys. Condens. Matter* **20**, 155203 (2008).

https://doi.org/10.1557/mrc.2017.107 Published online by Cambridge University Press